Pergamon

Acta mater. 49 (2001) 2887–2896

Acta MATERIALIA

www.elsevier.com/locate/actamat

PLASTICITY AND STRUCTURAL INSTABILITY IN A BULK METALLIC GLASS DEFORMED IN THE SUPERCOOLED LIQUID REGION

T. G. NIEH[1]†, J. WADSWORTH[1], C. T. LIU[2], T. OHKUBO[3] and Y. HIROTSU[3]

[1]Lawrence Livermore National Laboratory, L-350, PO Box 808, Livermore, CA 94551, USA, [2]Oak Ridge National Laboratory, Metals and Ceramics Division, Oak Ridge, TN 37831, USA and [3]The Institute of Scientific and Industrial Research, Osaka University, Osaka 567-0047, Japan

(Received 14 February 2001; received in revised form 23 May 2001; accepted 23 May 2001)

Abstract—The deformation behavior of a bulk amorphous Zr–10Al–5Ti–17.9Cu–14.6Ni alloy was characterized in the supercooled liquid region. The alloy was observed to exhibit Newtonian behavior at low strain rates but to become non-Newtonian at high strain rates. Structures of the amorphous material, both before and after deformation, were examined using X-ray diffraction and high-resolution electron microscopy. Experimental results showed the presence of nanocrystallites in the deformed samples, suggesting that the non-Newtonian behavior was associated with the concurrent crystallization of the amorphous structure during deformation; that is, a mixed crystalline-plus-amorphous structure was being tested. A mechanistic model based upon structural evolution has been developed to interpret the observed non-Newtonian behavior. © *2001 Acta Materialia Inc. Published by Elsevier Science Ltd. All rights reserved.*

Keywords: Metallic glasses; Superplasticity; Amorphous materials

1. INTRODUCTION

Intensive efforts have been carried out over the past decade to develop means to slow down the phase transformation kinetics during the forming of metallic glasses. As a result of these efforts, some bulk metallic glasses (BMGs) can now be fabricated from the liquid state at cooling rates of about 1–10 K s^{-1}, which are close to those of conventional casting. This enables the production of BMGs with a thickness over 10 mm. While advances in amorphous metallic alloy development have been impressive, they have been made largely through empirical developments [1].

Bulk amorphous alloys have many potential applications resulting from their unique properties, such as superior strength and hardness [2, 3], excellent corrosion resistance [4], shaping and forming in a viscous state [5, 6], reduced sliding friction and improved wear resistance [7], and low magnetic energy loss [8]. These properties should lead to applications in the fields of near-shape fabrication by injection molding and die casting, coatings, joining and bonding, biomedical implants, soft magnets for low energy loss, and synthesis of nanocrystalline and composite materials.

The mechanical behavior of BMGs can be classified by either inhomogeneous or homogeneous deformation. Inhomogeneous deformation usually occurs when a metallic glass is deformed at low temperatures (e.g. room temperature) and is characterized by the formation of localized shear bands, followed by rapid propagation of these bands, and catastrophic fracture. Consequently, when a metallic glass is deformed under tension it exhibits only limited macroscopic plasticity. Despite limited macroscopic plasticity, local strain within these shear bands can sometimes be quite significant. These bands are typically 20–30 nm in width and may be associated with deformation-induced crystallization [9] and even local melting [10]. Many different views exist on deformation mechanisms of inhomogeneous deformation in metallic glasses, and there is still no universal agreement.

Homogeneous deformation in metallic glasses usually takes place at high temperatures (>0.70 T_g, where T_g is the glass transition temperature), and the materials usually exhibit significant plasticity [11]. The transition temperature from the inhomogeneous to homogeneous deformation (or brittle-to-ductile transition) is strongly dependent upon strain rate. For example, for the $Zr_{65}Al_{10}Ni_{10}Cu_{15}$ alloy, the transition temperature is about 533 K (corresponding to 0.82

† To whom all correspondence should be addressed. Tel.: +1-925-4239802; fax: +1-925-4238034.
E-mail address: nieh1@llnl.gov (T. G. Nieh)

1359-6454/01/$20.00 © 2001 Acta Materialia Inc. Published by Elsevier Science Ltd. All rights reserved.
PII: S1359-6454(01)00218-X

T_g) at 5×10^{-4} s^{-1}, but it is 652 K (corresponding to 1.0 T_g) at 5×10^{-2} s^{-1} [12]. This rate dependence at the transition temperature suggests that homogeneous deformation is associated with some diffusional relaxation processes (even below T_g).

There is a growing interest in studying the homogeneous deformation of BMG, especially in the supercooled liquid region. This interest is, in part, stimulated by the fact that metallic glasses have excellent formability in this region, allowing net-shape forming. Several recent papers have been dedicated to the study of homogeneous deformation of BMG and a summary of some of the key observations is presented in Table 1.

Some of the papers in Table 1 are discussed here. Kawamura *et al.* [12] studied the high-temperature deformation of a $Zr_{65}Al_{10}Ni_{10}Cu_{15}$ metallic glass and found that, in the supercooled liquid region, plastic behavior was strongly dependent on strain rate. For each testing temperature, true Newtonian behavior, accompanied by high tensile elongations, was observed only in the low strain rate region. At high strain rates, the plastic flow became non-Newtonian, i.e. $m\neq1$, in equation $\dot{\varepsilon} = K\sigma^m$, where m is the strain rate sensitivity exponent, $\dot{\varepsilon}$ is the strain rate, σ is the flow stress, and K is a constant. The specific strain rate at which the transition occurred depends upon the testing temperature; specifically, the transition takes place at increasingly high strain rates as the testing temperature is reduced. The authors argued that the non-Newtonian behavior is associated with stress overshoot at high strain rate (or high stress), and that the stress overshoot was caused by a change in atomic mobility because of rapid deformation-induced change of free volume. However, no experimental evidence and, in particular, no structural information were presented in the paper.

Another similar study on the plastic flow of an amorphous $Zr_{55}Al_{10}Ni_5Cu_{30}$ alloy in the supercooled liquid region also indicated a transition from Newtonian to non-Newtonian behavior as strain rate increased [13]. In this case, the authors invoked the absolute reaction rate theory [14] to explain the observed increase in strain rate sensitivity with strain rate. However, it is pointed out that this theory is independent of the material structure; namely, it does not include structure parameters.

In summary, the deformation behavior of BMGs in the supercooled liquid region can be Newtonian viscous flow or non-Newtonian, depending upon testing temperature and strain rate. Nonetheless, large tensile ductilities are universally obtained in BMGs in the supercooled liquid region. In this paper, we offer another explanation for the observed non-Newtonian behavior from a structural point of view.

2. EXPERIMENTS

The material used in the present study has a composition of Zr–10Al–5Ti–17.9Cu–14.6Ni. Zone-purified Zr bars (containing 12.3 appm O and 10 appm Hf), together with pure metal elements, were used as charge materials. The alloys were prepared by arc melting in inert gas, followed by drop casting into Cu molds of diameter 6.4 mm and length 7.2 cm. The details of fabrication of the alloy have been described previously [10]. The glass transition temperature and the crystallization temperature (T_x) have been measured previously using differential scanning calorimetry (DSC) [15].

Tensile sheet specimens were fabricated from the as-cast material by means of electrical discharge machining. They had a gage length of 4.76 mm, a thickness of 1.27 mm and a width of 1.59 mm. Tensile tests were conducted using an Instron machine equipped with an air furnace. To minimize crystallization during testing, a fast heating rate was used. Typically, the heating-plus-holding time prior to testing was about 25 min. For example, for a test at 410°C at a constant strain rate of 10^{-2} s^{-1}, the temperature profile was: 305°C (5 min), 371°C (10 min), 397°C (15 min), 407°C (20 min), 410°C (23 min), and 410°C (24 min). Constant strain rate tests were performed with a computer-controlled machine within a temperature range of 663–743 K at a constant strain rate of 10^{-2} s^{-1}. To measure strain rate sensitivity exponents, both strain rate decrease and strain rate increase tests were performed.

Samples tested in air in the supercooled liquid region generally oxidized. To prevent sample oxidation, some tests were also conducted in a quartz tube, which was evacuated to a vacuum of 10^{-3} Pa. A test sample was heated indirectly by a suscepter, which was heated directly by induction heating. Two thermocouples, one attached to the end and another to the center of the tensile specimen, were used to monitor testing temperature. In this case, constant cross-head speed tests were performed at tempera-

Table 1. Summary of the deformation data of some metallic glasses in the supercooled liquid region

Alloys	T_g/T_x, K	Strain rate, s^{-1}	m	Elongation	Ref.
$Pd_{78.1}Fe_{5.1}Si_{16}$	668/683	~0.5	~1.0	N/A	[28]
$Co_{68}Fe_7Ni_{13}Si_7B_5$	836/856	10^{-2}	N/A	180	[29]
$Ni_{77.5}Si_{7.5}B_{15}$	N/A	N/A	1.09	N/A	[30]
$La_{55}Al_{25}Ni_{20}$	480/520	10^{-4}–10^{0}	1	1800	[31]
$Zr_{65}Al_{10}Ni_{10}Cu_{15}$	652/757	10^{-4}–10^{-1}	<0.8	340	[12]
$Pd_{40}Ni_{40}P_{20}$	578/651	10^{-4}–10^{0}	1.0	N/A	[12]
$Zr_{55}Al_{10}Ni_5Cu_{30}$	685/763	$<10^{-4}$	1.0	N/A	[13]
$Zr_{52.5}Al_{10}Ti_5Cu_{17.9}Ni_{14.6}$	631/729	10^{-2}	~0.65	650	[32]

tures of 683–713 K (within the supercooled liquid region) at strain rates of 10^{-2} and 10^{-3} s^{-1}.

Microstructural evolution in the deformed specimens was also examined using a high-resolution electron microscope (JEM-3000F model, operated at 300 kV). Areas near the grip and in the vicinity of the fracture tip of the tested specimens were examined. For the grip area, the sample was mechanically thinned in water and then ion-milled using a liquid-nitrogen specimen cooling stage. For the areas near the tip of the fractured samples, on the other hand, transmission electron microscopy (TEM) observations were carried out directly without additional thinning.

3. MECHANICAL PROPERTIES

The stress–strain behavior of the Zr–10Al–5Ti–17.9Cu–14.6Ni alloy at different temperatures at a strain rate of 10^{-2} s^{-1} is shown in Fig. 1. A yield drop (or stress overshoot) phenomenon is readily observed at low temperatures, and in particular at 663 and 683 K. The yield drop is very dramatic. For example, at 663 K the yield drop is 750 MPa (i.e. from 1600 MPa to 850 MPa), which is about the same magnitude as its flow strength (~850 MPa). The yield drop phenomenon has also been reported previously in $Zr_{65}Al_{10}Ni_{10}Cu_{15}$ [16] and $Zr_{55}Al_{10}Ni_5Cu_{30}$ [13] in the supercooled liquid region. Chen *et al.* [17] argued that the yield drop was a result of rapid increase in free volume during high strain rate deformation. Upon yielding, the excessive free volume quickly redistributed via local atomic rearrangement and results in the observed yield drop. Kawamura *et al.* [16] demonstrated that the magnitude of yield drop depends on testing temperature and strain rate. Since the creation of excessive free volume and the subsequent annihilation are kinetic processes, it is not surprising that the yield drop is both temperature and rate dependent.

The yield drop phenomenon is noted to disappear at high temperatures (>683 K), as shown in Fig. 1.

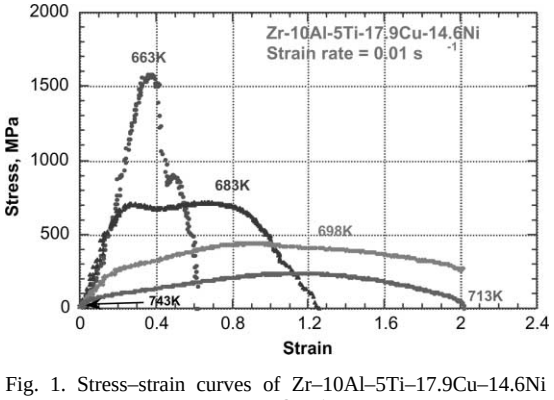

Fig. 1. Stress–strain curves of Zr–10Al–5Ti–17.9Cu–14.6Ni obtained at a strain rate of 10^{-2} s^{-1} and temperatures within the supercooled liquid region. The yield drop phenomenon is readily seen, especially at low temperatures.

At these temperatures, there is an initial hardening, followed by a gradual decrease in flow stress until final fracture. As shown in Fig. 1, the fracture strain increases with increasing test temperature and reaches a maximum value of about 2.0 (~650% elongation) at 698 and 713 K. At 743 K, which is above the crystallization temperature (729 K), the alloy becomes completely brittle. It is noted that samples which were deformed in the supercooled liquid region exhibit gradual necking. In fact, some samples necked down nearly to a point. The final decrease in flow stress is not, therefore, a result of softening but of reduction in load bearing area. This is in contrast to the previous observation, in which uniform deformation was observed in a $Zr_{65}Al_{10}Ni_{10}Cu_{15}$ metallic glass [18]. The difference may be caused by the fact that the samples used in this study were very thin (0.5 mm). As a result, the samples were deformed under a plane-stress condition. In the case of testing a thick specimen, there is a stress distribution within the specimen, even though it is under uniaxial tension. Since metallic glasses generally exhibit high strain rate sensitivity in the supercooled liquid region, the deformation rate would be relatively non-uniform in a thick testing sample. This leads to preferential necking and thus reduced elongation. However, a thin testing specimen is comparatively less susceptible to stress/strain rate non-uniformity during deformation.

It is evident in Fig. 1 that both the flow stress and fracture strain are extremely sensitive to the testing temperature. For example, with only a 15 K difference in testing temperature, the flow stress drops from 700 MPa at 683 K to about 400 MPa at 698 K, but the tensile elongation is almost tripled (230% to 630%). The flow stresses are noted to be relatively high; for example, at even 713 K the flow stress is about 200 MPa. This value is considerably higher than the flow stresses generally measured in metals or ceramics exhibiting superplasticity or extended ductility [19]. Flow stresses for superplastic metals or ceramics are typically lower than 35 MPa.

To characterize the deformation behavior, both strain rate decrease (Fig. 2) and increase (Fig. 3) tests were performed at 683 K. Several observations are worth noting in Figs. 2 and 3. To minimize structural instability, i.e. the occurrence of structural crystallization, testing parameters were chosen so that tests were conducted within the shortest time possible. Therefore, a strain interval of 0.08 was chosen between each strain rate change during the strain rate decrease test (Fig. 2). Also, strain rates were carefully chosen to avoid stress overshoot. Stress overshoot does not take place at strain rates lower than 9×10^{-3} s^{-1}, as shown in Fig. 2. Despite these precautions, it is still pointed out that data at a plastic strain of over 0.8 are less reliable because of possible structural changes in the testing sample as a result of prolonged thermal exposure under stress. For example, the peculiar increase in the flow stress (strain hardening) at a relatively slow strain rate of 2.8×10^{-4} s^{-1} is revealed

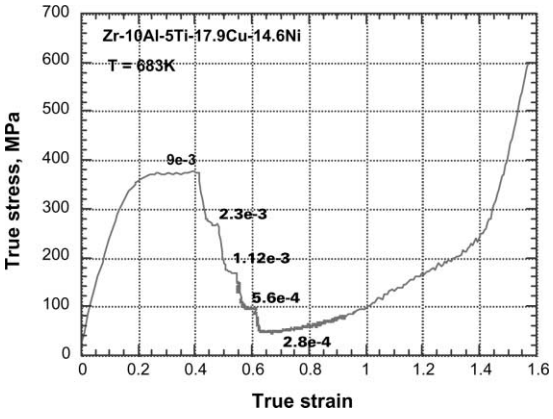

Fig. 2. Strain rate decrease tests on Zr–10Al–5Ti–17.9Cu–14.6Ni performed at 683 K. A monotonic increase in flow stress after the final rate reduction is caused by concurrent nanocrystallization during testing.

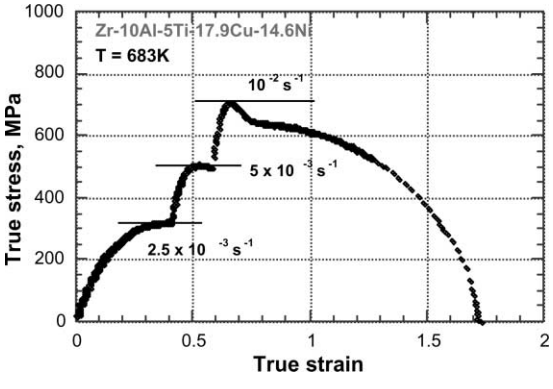

Fig. 3. Strain rate increase tests on Zr–10Al–5Ti–17.9Cu–14.6Ni performed at 683 K.

in Fig. 2. This is in fact associated with structural change, as will be demonstrated in a subsequent section.

For the strain rate increase test, the starting strain rate was chosen to be sufficiently high to minimize structural change, but not too high to result in a stress overshoot. Despite these precautions, stress overshoot was still observed at a strain rate of 10^{-2} s^{-1} (Fig. 3). However, we use the "steady state" value as the flow stress for subsequent analysis.

Using data from both Figs 2 and 3, a logarithm stress–logarithm strain rate plot is produced, as shown in Fig. 4. The value of strain rate sensitivity *m* is found to vary with strain rate. Specifically, the strain rate decrease test produces an *m* value close to unity in the low strain rate range ($<10^{-3}$ s^{-1}). However, it decreases with increasing strain rate, and is much less than unity in the high strain rate range ($>10^{-3}$ s^{-1}). In comparison, the strain rate increase test yields slightly higher flow stresses and *m* values. This may be caused by a temperature drift in the test. As indicated previously, the flow stress is extremely sensitive to testing temperature. However, the *m* value, although measured only from the high strain rate range, is

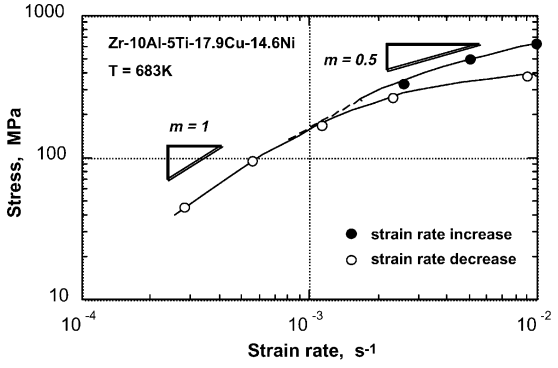

Fig. 4. Stress–strain rate relationship for Zr–10Al–5Ti–17.9Cu–14.6Ni at 683 K. The strain rate sensitivity exponent, *m*, varies with strain rate.

much less than unity, indicating non-Newtonian behavior. In summary, both strain rate change tests show that plastic flow is non-Newtonian in the high strain rate range.

4. STRUCTURAL AND FRACTURE ANALYSES

In the present study, tensile tests were initially performed in air which resulted in serious sample oxidation [20]. This created some difficulties for structural analysis and sample preparation using X-ray and TEM. For example, the presence of X-ray diffraction peaks may be simply indicative of oxide formation. To prepare clean samples for structural analyses, several tensile tests were subsequently conducted in vacuum. Although it is known that the presence of oxygen can have a detrimental effect on the amorphization of a metallic glass [21], our test results indicated that there was no significant difference between data obtained in air or vacuum [22]. This conclusion is consistent with the previous observation of Liu *et al.* [10].

To further shed light on microstructural changes during deformation, high-resolution electron microscopy (HREM) was employed to examine samples both before and after deformation. The microstructure of the as-cast sample is shown in Fig. 5. It is essentially featureless, although some local chemical ordering has been detected [23]. Upon thermal exposure at 683 K, which is slightly above the glass transition temperature, no microstructural change was discernible. Specifically, no local nanocrystalline region could be found. This is demonstrated in Fig. 6, which is an image taken from the grip section of a sample tested at the temperature. In the figure, a selected-area electron diffraction (SAED) pattern is also included in the inset. The HREM image and the SAED halo-pattern clearly indicate that the microstructure remains amorphous after static annealing at 683 K.

Nanocrystallization was observed to occur at the region near the fracture tip of a sample tested at 683 K. A typical TEM image taken from the region is

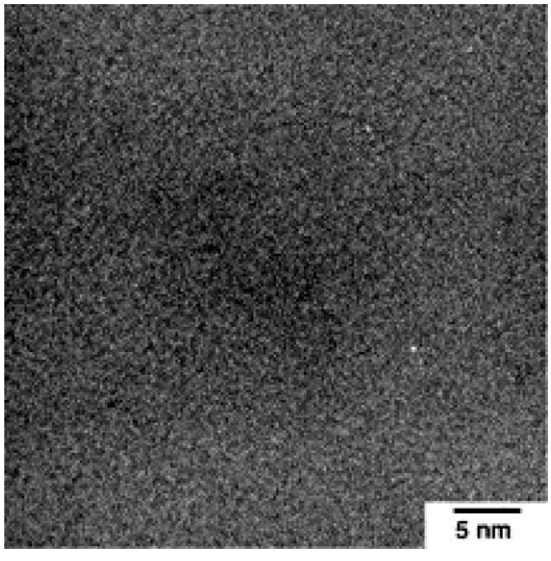

Fig. 5. Transmission electron micrograph showing the amorphous nature of the alloy in the as-cast state.

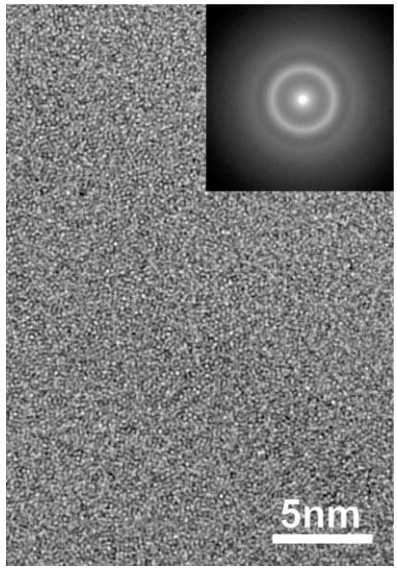

Fig. 6. HREM image showing the structure from the grip region of the amorphous Zr–10Al–5Ti–17.9Cu–14.6Ni sample deformed at 683 K at a strain rate of 10^{-2} s^{-1}.

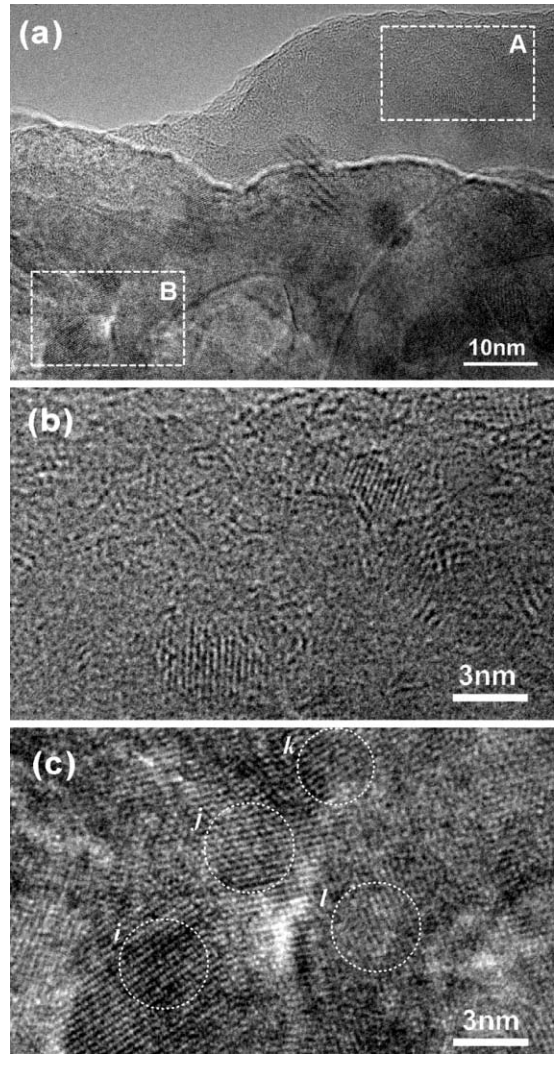

Fig. 7. (a) Typical TEM image from the fracture tip of the amorphous Zr–10Al–5Ti–17.9Cu–14.6Ni sample deformed at 683 K at a strain rate of 10^{-2} s^{-1}. (b) High magnification of area A in (a) showing individual nanocrystals (~3 nm) dispersed in an amorphous matrix. (c) High magnification of area B in (a) showing aggregates of nanocrystallites (~5–10 nm).

shown in Fig. 7a. Figures 7b and 7c are HREM images taken from the regions A and B in Fig. 7a, respectively. The structure in Fig. 7a reveals two different morphologies. One morphology has an amorphous-like matrix but contains areas with local lattice fringes extending as small as 3 nm (Fig. 7b). Another morphology is composed of an aggregate of nanosized (~5–10 nm) crystallites. The sizes of these crystallites are as small as 10 nm, similar to the size estimated from an X-ray diffraction study reported previously [22]. To investigate these crystallites, SAED was performed. The patterns i, j, k, l in Fig. 8a are SAED from the encircled areas denoted i, j, k, l in Fig. 7c, respectively, illustrating the mutual orientations of these nanograins. The relative orientations between these nanocrystallites are apparently not low-angle. From the SAED patterns in Fig. 7c, one can readily perform Fourier transformation for crystal structure analysis (Fig. 8b). A set of Fourier transformed patterns, as shown in Fig. 8c, can all be indexed by the structures of Zr_2Ni and Zr_2Cu. This is consistent with previous observations [15]. It is noted that we also observed regions of fully amorphous structure (without any local lattice fringes) immediately adjacent to the nanocrystalline regions. Figure 9 shows an HREM image of such a region with a halo SAED pattern in the inset.

The microstructure from the grip region of the sample deformed at 713 K shows finely dispersed nanocrystals dispersed in an amorphous matrix, as shown

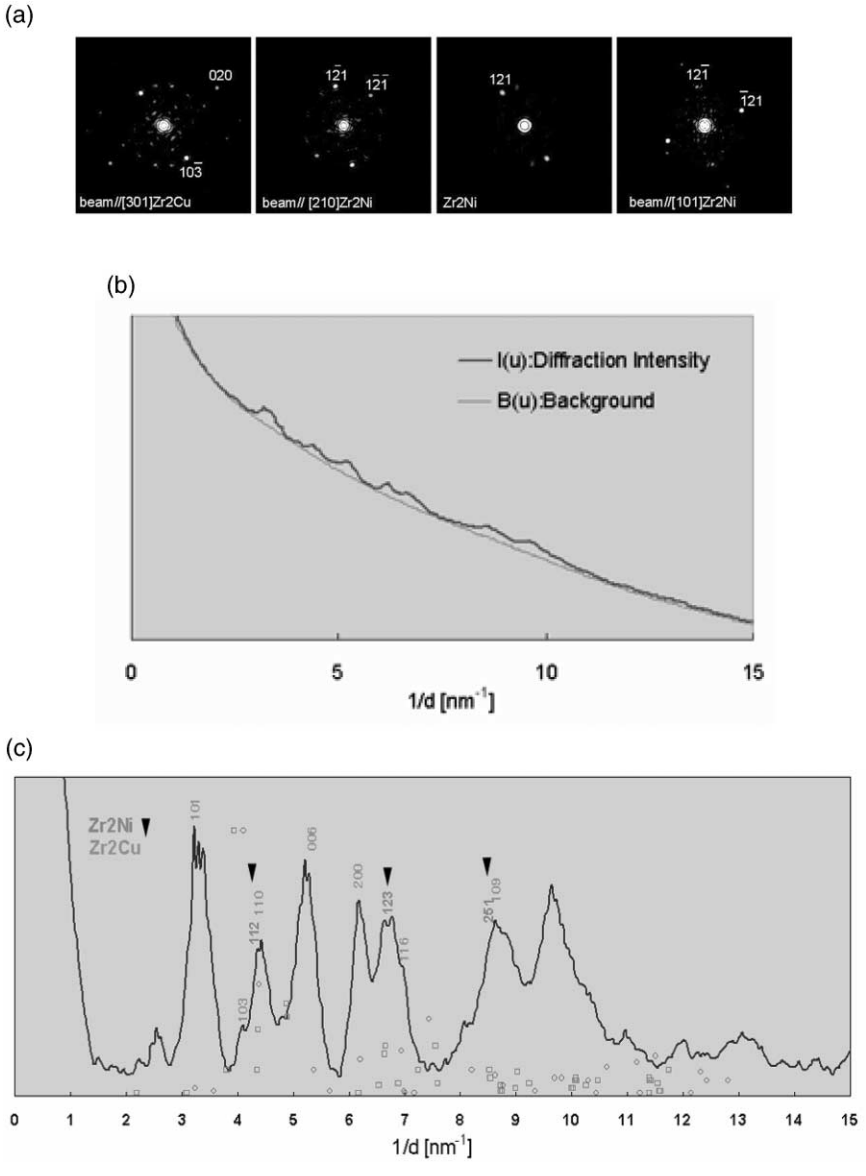

Fig. 8. (a) SAED patterns from various regions in Fig. 7c; (b) Fourier transformed pattern deduced from intensity and background profiles; (c) Fourier transformed pattern indexed by the structures of Zr_2Ni and Zr_2Cu.

in Fig. 10. In the figure, an SAED pattern consisting of spotty diffraction rings with a diffuse background from the amorphous matrix is also included in the inset. The pattern indicates that the atomic planes in the nanocrystals embedded in the amorphous matrix are not greatly deformed. An HREM image of the nanocrystalline structure from the thin region in Fig. 10 is shown in Fig. 11. The image shows regions with clear lattice fringes in an amorphous matrix, which is consistent with the SAED information.

It is well documented that the typical fracture surfaces of metallic glasses exhibit vein patterns at room temperature, as a result of the sudden release of elastic energy at fracture. Also, the material has no local necking resistance. In contrast, in the supercooled liquid region, a metallic glass shows strong resistance to local necking, as a result of the high strain rate sensitivity. The fracture surface of the sample tested at 663 K and at a strain rate of 10^{-2} s^{-1} is shown in Fig. 12. It appears that a vein pattern persists even at 663 K (above T_g). However, the vein pattern is quite different from that observed at room temperature; specifically, the ridges between voids are much higher and there is no indication of melting droplets. Large voids are also present. These voids develop under triaxial stresses prior to the final fracture of the sample. As discussed previously, samples deformed in the supercooled liquid region exhibit considerable necking. The reduction in area for the 663 K sample was about 96%. At 683 K, the sample fractured nearly to a chisel point (reduction in area = 99%). The fracture surface (Fig. 13) in the 683 K sample reveals ductile

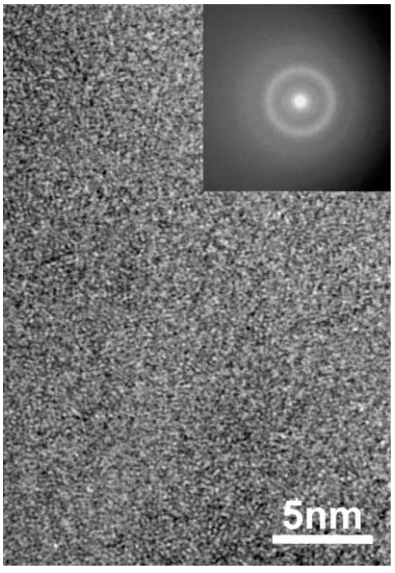

Fig. 9. HREM image showing regions of fully amorphous structure immediately adjacent to the nanocrystalline region.

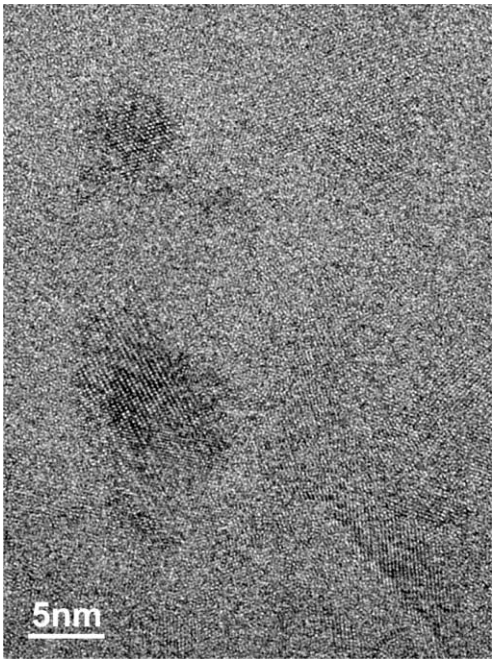

Fig. 11. HREM image from the thin region in Fig. 9.

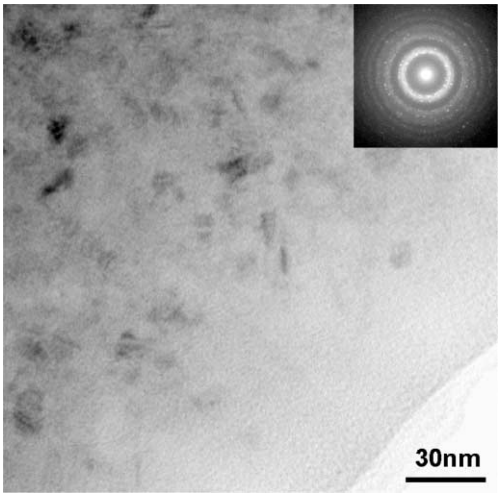

Fig. 10. TEM image from the grip region of the Zr–10Al–5Ti–17.9Cu–14.6Ni sample deformed at 713 K at a strain rate of 10^{-2} s^{-1} showing the occurrence of nanocrystallization.

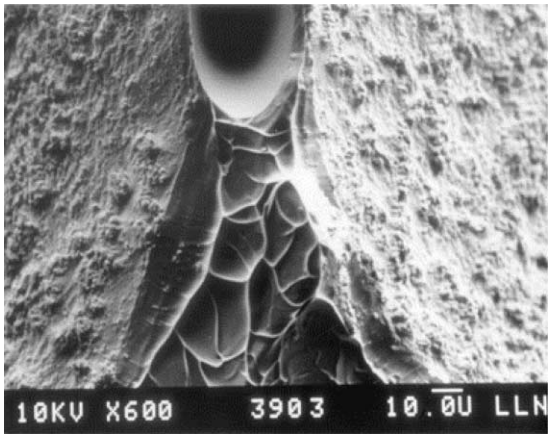

Fig. 12. Fracture surface of the sample tested at 663 K and at a strain rate of 10^{-2} s^{-1}.

dimples and there is no indication of a vein pattern. The brittle-to-ductile transition from inhomogeneous to homogeneous deformation is clearly revealed by the fracture surface appearance.

5. DISCUSSION

The present study shows that the observed non-Newtonian behavior in the Zr–10Al–5Ti–17.9Cu–14.6Ni alloy at high strain rates is attributable to concurrent nanocrystallization during deformation. On the other hand, other studies [12, 17] suggested that the non-Newtonian behavior was associated with stress overshoot at high strain rate (or high stress), and the stress overshoot was caused by a change in atomic mobility due to rapid deformation-induced change of free volume. It is noted that both nanocrystallization and free volume creation are kinetic processes, which are temperature and strain rate dependent. Therefore, it is not surprising to observe the presence of both Newtonian and non-Newtonian flows in the same materials but at different temperature and strain rate regimes. The present study, as well as others [12, 13], indicates that a high strain rate and low temperature (i.e. near the glass transition temperature) condition favors non-Newtonian flow.

As discussed above, nanocrystallization takes place in the present alloy during deformation in the supercooled liquid region, especially in the high strain rate range ($>10^{-3}$ s^{-1}). The nanocrystallization is a dynamic process, i.e. it is stress as well as tempera-

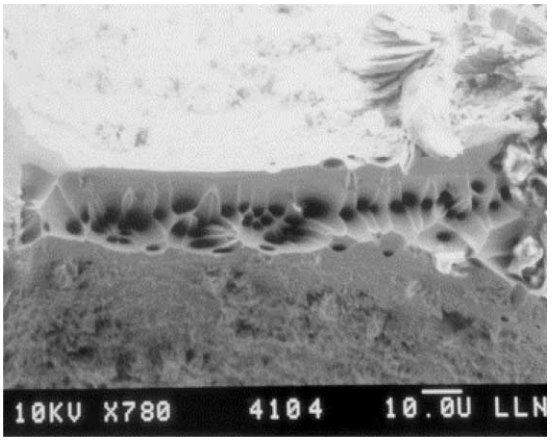

Fig. 13. Fracture surface of the sample tested at 683 K and at a strain rate of 10^{-2} s^{-1} revealing a ductile dimple appearance with no evidence of a vein pattern.

ture driven. The presence of nanocrystalline phases can significantly affect the mechanical properties of a metallic glass. For example, Busch and Johnson [24] recently showed that the presence of crystalline phases increases the viscosity of amorphous $Zr_{46.75}Ti_{8.25}Cu_{7.5}Ni_{10}Be_{27.5}$ alloy. Kim *et al.* [25, 26] also reported that the strength of amorphous $Al_{88}Ni_{10}Y_2$ was doubled when the alloy was partially crystallized and contained Al particles of size 5–12 nm. The fact that the strength of an amorphous alloy is increased by the presence of nanocrystalline particles can be used to explain the flow stress increase after the final strain rate reduction, as illustrated in Fig. 2. In this case, the flow stress monotonically increases as a result of increasing concentration of nanocrystalline phases. In the following, we discuss the effect of the presence of nanocrystallites in a metallic glass on its mechanical behavior.

It is noted that ideal Newtonian viscous flow is an exception rather than the rule in flow of viscous materials [27]. From a rheological viewpoint, the shear strain rate of a glass, $\dot{\gamma}$, is a nonlinear function of applied shear stress, τ, i.e.

$$\dot{\gamma} = f(\tau) \tag{1}$$

Assuming convergence, equation (1) can be mathematically expanded into a Taylor series:

$$\dot{\gamma} = \sum_{i=1}^{n} A_i \tau^i = A_1\tau + A_2\tau^2 + A_3\tau^3 + A_4\tau^4 + A_5\tau^5 + \ldots \tag{2}$$

Each term in the above series has its own physical mechanism and can be identified with a specific, high-temperature, deformation process in polycrystalline solids. The first term ($A_1 \neq 0$) represents *ideal* Newtonian viscous flow. The second term ($A_2 \neq 0$) represents a grain-boundary sliding mechanism commonly observed in fine-grained, crystalline, superplastic materials. The third term ($A_3 \neq 0$) represents a deformation process controlled by viscous glide of dislocations in a crystalline lattice. The fourth term ($A_4 \neq 0$) represents a deformation process controlled by dislocation climb in a crystalline lattice. The non-zero values of the other $A_i\tau^i$ where $i>5$ represent higher-order deformation mechanisms, such as the particle strengthening that is often observed in heavily alloyed materials or structural composites.

The intrinsic tensile ductility associated with each deformation mechanism is different. In principle, the ductility decreases with increasing i value; this is attributed to decreased neck stability under tensile deformation, as a result of decreased strain rate sensitivity. For an ideal Newtonian fluid, the ductility is in theory unlimited. In practice, however, the ductility achieved experimentally is limited by constraints such as the length of the testing furnace, and the uniformity of the hot zone. The intervention of the other mechanisms, as listed in Table 2, can then further reduce the tensile ductility.

The respective order of equation (2) is not universal but determined by the alloy system, the test temperature, strain rate, and the microstructure of the material. For example, as shown above, the present metallic glass does not behave like an ideal Newtonian fluid in the high strain rate range because of the concurrent operation of other deformation mechanisms resulting from the partial nanocrystallization of the amorphous structure. The presence of these new fine-crystal regions would be expected to modify the Newtonian behavior. For example, if an alloy contains aggregates of nanocrystalline grains (Fig. 7c), having a mixed nanocrystalline-plus-amorphous structure, as shown schematically in Fig. 14a, then to a first approximation the total deformation rate can be expressed by:

$$\dot{\gamma}_{total} = (1-f_v)\dot{\gamma}_{am} + f_v\dot{\gamma}_{cry} \tag{3}$$

where $\dot{\gamma}_{total}$ is the total strain rate, $\dot{\gamma}_{am}$ and $\dot{\gamma}_{cry}$ are the strain rates resulting from the amorphous and crystalline phases, respectively, and f_v is the volume fraction of the crystalline phase. Since the plastic flow of an amorphous alloy can be described by $\dot{\gamma}_{am} = A\tau$, and the plastic flow of a nanocrystalline, superplastic alloy can be described by $\dot{\gamma}_{cry} = B\tau^2$ where τ is the flow stress, and A and B are material constants, equation (3) becomes:

$$\dot{\gamma}_{total} = (1-f_v)A\tau + f_v B\tau^2 \tag{4}$$

It is obvious from equation (4) that the measured strain rate sensitivity would have to fall between 0.5, the value for grain boundary sliding in fine-grained

Table 2. Different deformation mechanisms, and the approximate ductility associated with each term in equation (2)

Coefficient	Mechanism	Approximate expected maximum elongation, e
A_1	Newtonian viscous flow	unlimited
A_2	Grain-boundary sliding	300%<e<8000%
A_3	Viscous dislocation glide	50%<e<300%
A_4	Dislocation climb	e<50%
A_5, A_6, A_7, ….	Particle strengthening	e<10%

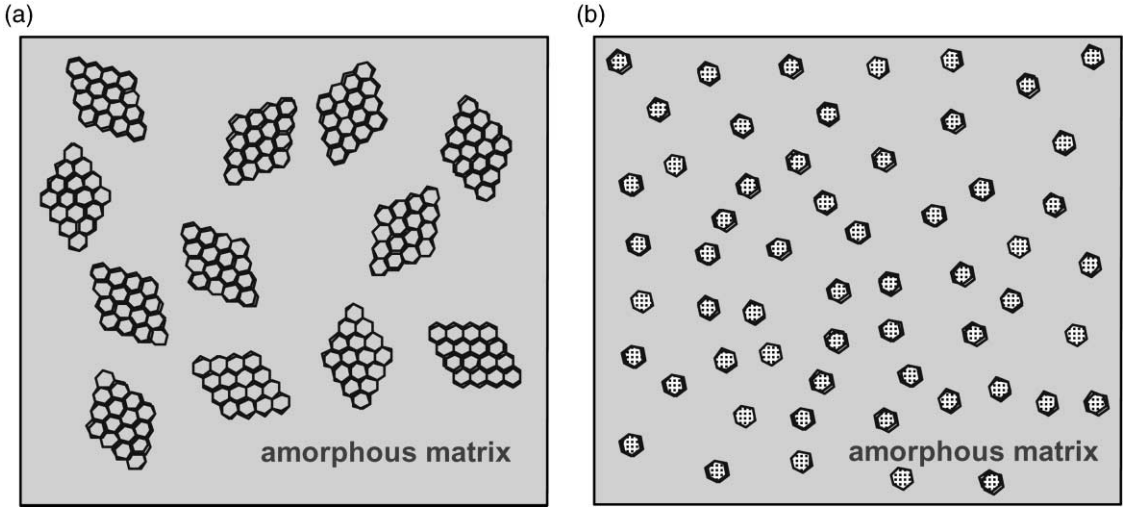

Fig. 14. Nanocrystallization of an amorphous alloy produces two types of nanocrystalline morphologies: (a) crystalline aggregates; (b) isolated crystals.

crystalline material, and unity, the value for Newtonian viscous flow.

However, if an alloy contains isolated nanocrystalline grains in an amorphous matrix (Figs 7b and 14b), instead of having regions of nanocrystalline grains, the total deformation rate can now be expressed by:

$$\dot{\gamma}_{\text{total}} = (1-f_v)A\tau + f_v B\tau^n \qquad (5)$$

where n>5, because the crystalline region of the material is treated as a dispersion strengthened solid. Obviously, the overall stress exponent for this alloy is also greater than unity, i.e. m<1, but is not bounded at a lower level by $m = 0.5$ as in the case for the example of region of nanocrystalline grains.

Of additional interest is the drastic decrease in tensile elongation in BMG at temperatures immediately above the crystallization temperature. For example, when a $Zr_{52.5}Al_{10}Ti_5Cu_{17.9}Ni_{14.6}$ alloy ($T_x = 729$ K) was tested at 743 K (Fig. 1), the alloy exhibits almost zero ductility. This appears to be contrary to the conventional wisdom that a nanograined alloy is expected to exhibit large elongations, presumably resulting from extensive grain boundary sliding. However, it must be pointed out that in the case of grain boundary sliding the sliding strain must be accommodated either by diffusional flow or by dislocation slip (e.g. climb or glide) across neighboring grains to prevent cavitation and fracture; this is illustrated schematically in Fig. 15. Dislocation slip in a multicomponent, ordered intermetallic compound is not expected to be easy even at temperatures near T_x (~0.8 T_m, where T_m is the melting point of the alloy).

On the other hand, when the grain size is sufficiently small, e.g. in the nanometer range, the dif-

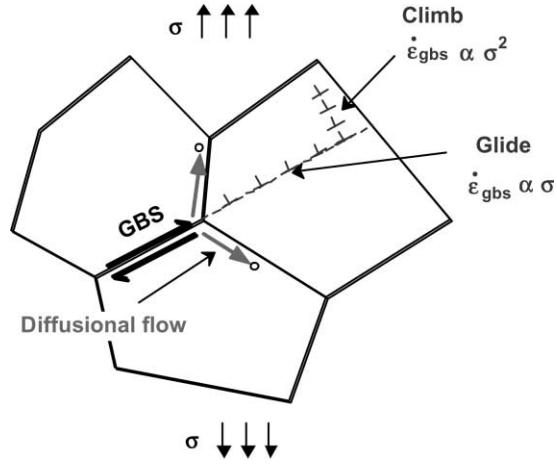

Fig. 15. Strain accommodation is necessary at grain triple junctions to prevent cavitation, which leads to fracture during superplastic deformation of fine-grained materials. The accommodation can take place through either a slip or a diffusional process.

fusion distance that is required for accommodation is also short. (Diffusional distance is estimated to be of the same scale as the grain size.) In such a case, the possibility of diffusional accommodation must also be considered. The criterion for the prevalence of diffusional accommodation can be estimated using the equation:

$$\sqrt{D_b t} > d \tag{6}$$

where D_b is the grain-boundary self diffusivity, t is the time, and d is the grain size. Obviously, this equation favors a small grain size, a slow strain rate, and fast diffusivity. If the diffusional process is not sufficiently fast to accommodate the sliding strain, especially at high strain rates, cavitation would take place and fracture follows. This accounts for the low tensile elongation in some metallic glasses even though they show a high m value at temperatures in the vicinity of T_x.

6. SUMMARY

Plastic flow of a bulk amorphous Zr–10Al–5Ti–17.9Cu–14.6Ni alloy was characterized in the supercooled liquid region. The alloy has excellent mechanical formability in the supercooled liquid region. The alloy exhibited Newtonian behavior at low strain rates, but became non-Newtonian as the strain rate increases. Microstructural examinations showed that even though tests were carried out in the supercooled liquid region, nanocrystallization still took place. Although the structure in the grip region remained amorphous, nanocrystallization occurred in the deformed region, indicating that nanocrystallization was stress driven. Therefore, the observed non-Newtonian behavior can be attributed to glass instability during deformation. Composite models were presented to explain the strain rate sensitivity values. Multicomponent BMG can be used as a precursor for nanocrystalline solids; however, nanocrystalline solids are not necessarily superplastic. The non-superplastic behavior is caused by the difficulty of strain accommodation at grain triple junctions.

Acknowledgements—This work was performed under the auspices of the US Department of Energy (DOE) under contract No. W-7405-Eng-48 with Lawrence Livermore National Laboratory and, in part, was supported by the Division of Materials Science and Engineering, Office of Basic Science, US Department of Energy under contract No. W-7405-Eng-48 with Lawrence Livermore National Laboratory and under contract No. DE-AC05-00OR22725 with Oak Ridge National Laboratory managed by UT-Battelle, LLC.

REFERENCES

1. Johnson, W. L., *MRS Bull.*, 1999, **24**(10), 42.
2. Inoue, A., Kimura, H. M., Sasamori, K. and Masumoto, T., *Mater. Trans. JIM*, 1994, **35**(2), 85.
3. Hays, C. C., Kim, C. P. and Johnson, W. L., *Phys. Rev. Lett.*, 2000, **84**(13), 2901.
4. Hashimoto, K., in *Current Topics in Amorphous Materials: Physics and Technology*, ed. Y. Sakurai, Y. Hamakawa, T. Masumoto, K. Shirae and K. Suzuki. Elsevier Science Publishers B.V, 1993, p. 167.
5. Kawamura, Y., Shibata, T., Inoue, A. and Masumoto, T., *Appl. Phys. Lett.*, 1996, **69**(9), 1208.
6. Kawamura, Y., Shibata, T., Inoue, A. and Masumoto, T., *Acta mater.*, 1998, **46**(1), 253.
7. Wang, J. G., Choi, B. W., Nieh, T. G. and Liu, C. T., *J. Mater. Res.*, 2000, **15**(4), 913.
8. Inoue, A., Miyauchi, Y. and Masumoto, T., *Mater. Trans. JIM*, 1995, **36**(5), 689.
9. Chen, H., He, Y., Shiflet, G. J. and Poon, S. J., *Nature*, 1994, **367**(6463), 541.
10. Liu, C. T., Heatherly, L., Easton, D. S., Carmichael, C. A., Schneibel, J. H., Chen, C. H. *et al.*, *Metall. Mater. Trans. A*, 1998, **29A**(7), 1811.
11. Argon, A. S., *Acta metall.*, 1979, **27**, 47.
12. Kawamura, Y., Nakamura, T. and Inoue, A., *Scripta mater.*, 1998, **39**(3), 301.
13. Reger-Leonhard, A., Heilmaier, M. and Eckert, J., *Scripta mater.*, 2000, **43**, 459.
14. Eyring, H., *J. Chem. Phys.*, 1936, **4**, 283.
15. Wang, J. G., Choi, B. W., Nieh, T. G. and Liu, C. T., *J. Mater. Res.*, 2000, **15**(3), 798.
16. Kawamura, Y., Shibata, T., Inoue, A. and Masumoto, T., *Mater. Trans. JIM*, 1999, **40**(4), 335.
17. Chen, H. S., Kato, H. and Inoue, A., *Mater. Trans. JIM*, 2001, **42**(4), 597.
18. Kawamura, Y., Shibata, T. and Inoue, A., *Scripta mater.*, 1997, **37**(4), 431.
19. Nieh, T. G., Sherby, O. D. and Wadsworth, J., *Superplasticity in Metals and Ceramics*. Cambridge University Press, Cambridge, UK, 1997.
20. Wadsworth, J. and Nieh, T. G., in *Superplasticity—Past, Present, and Future, MRS Symp. No. 601*, ed. P. Berbon, M. Berbon, T. G. Langdon and T. Sakuma. Materials Research Society, Pittsburgh, PA, 2000, p. 141.
21. Lin, X. H., Johnson, W. L. and Rhim, W. K., *Mater. Trans. JIM*, 1997, **38**(5), 473.
22. Nieh, T. G., Wadsworth, J., Liu, C. T., Ice, G. E. and Chung, K. -S., *Mater. Trans. JIM*, 2001, **42**(4), 613.
23. Asoka-Kumar, P., Hartley, J., Howell, R., Sterne, P. A. and Nieh, T. G., *Appl. Phys. Lett.*, 2000, **77**(13), 1973.
24. Busch, R. and Johnson, W. L., *Appl. Phys. Lett.*, 1998, **72**(21), 2695.
25. Kim, Y. H., Inoue, A. and Masumoto, T., *Mater. Trans. JIM*, 1990, **31**, 747.
26. Kim, Y. H., Hiraga, K., Inoue, A., Masumoto, T. and Jo, H. H., *Mater. Trans. JIM*, 1994, **35**(5), 293.
27. Chhabra, R. P., *Bubbles, Drops, and Particles in Non-Newtonian Fluids*. CRC Press, Boca Raton, Florida, 1993.
28. Homer, C. and Eberhardt, A., *Scripta metall.*, 1980, **14**, 1331.
29. Zelenskiy, V. A., Tikhonov, A. S. and Kobylkin, A. N., *Russian Metall.*, 1985, **4**, 152.
30. Csach, K., Fursova, Y. V., Khonik, V. A. and Ocelik, V., *Scripta mater.*, 1998, **39**(10), 1377.
31. Kawamura, Y., Nakamura, T., Inoue, A. and Masumoto, T., *Mater. Trans. JIM*, 1999, **40**(8), 794.
32. Nieh, T. G., Mukai, T., Liu, C. T. and Wadsworth, J., *Scripta mater.*, 1999, **40**(9), 1021.